Sustainable Energy & Fuels

ROYAL SOCIETY OF CHEMISTRY

REVIEW

View Article Online
View Journal | View Issue

Cite this: *Sustainable Energy Fuels*, 2025, **9**, 323

Empowering catalysis and separation: morphology control of MFI zeolites using organic additives

Jun Zhao,[ab] Haijun Yu,[ab] Haimei Xu,[b] Zhiyu He,[a] Feng Shao,*[a] Peng Lu*[b] and Valentin Valtchev*[bc]

As one of the most successful inorganic materials, MFI zeolite has been widely used in petrochemical and fine chemical industries. However, the presence of only micropores in MFI zeolite creates diffusion barriers and thus precludes its usage in processes involving large substrates. It is highly desirable to mitigate the diffusion pathways in MFI zeolites. One of the efficient methods is the morphology control strategy, which has become a hot topic in the past few decades. In this review, we summarize the progress of MFI zeolite morphology control using specific organic additives as morphology modifiers to enhance the catalytic and separation performance. Organic additives, including urea, amino acids, small organic molecules, and polymers, were categorized based on the MFI zeolites induced by them. The morphologies generated can be classified as nanocrystals, aggregated nanoparticles, nanosheets, intergrown nanosheets, plates, intergrown plates, needles, and bulky prismatic crystals, depending on the specific additives. The formation mechanisms of different morphological MFI zeolites and their properties are also discussed. This review is of great importance for the controllable synthesis of zeolites and rational design of zeolite catalysts.

Received 30th October 2024
Accepted 1st December 2024

DOI: 10.1039/d4se01514b

rsc.li/sustainable-energy

1. Introduction

Zeolites, one of the most important inorganic microporous materials with a plethora of applications such as ion-exchangers, adsorbents, and catalysts,[1–7] are constructed from tetrahedral atoms (T-atoms, such as Si, Al, and P) bridged by oxygen atoms to form three-dimensional frameworks. Uniform-sized micropores and high thermal and hydrothermal stability provide zeolites with excellent properties, especially as molecular sieves for size-related processes. MFI zeolite, a "star zeolite", has been used extensively in petrochemical and fine chemical industries. The structure of MFI zeolite comprises two-channel systems, *i.e.*, a sinusoidal channel (5.1 × 5.5 Å) along the *a*–*c* direction and a straight channel (5.4 × 5.6 Å) along the *b*-axis.[8–10] According to its framework compositions, MFI zeolite subtypes mainly include ZSM-5 (aluminosilicate),[11] silicalite-1 (silicate),[12] TS-1 (titanosilicate),[13] *etc.* ZSM-5 was the first zeolite with MFI topology to be reported in the 1970s by Mobil.[14] Based on their compositions, ZSM-5, silicalite-1, and TS-1 are widely used as acidic catalysts, adsorbents/membranes, and oxidation catalysts, respectively.

Due to their microporous nature, MFI zeolites showed limitations in processes involving large substrates, thus hindering their potential applications. Strategies for mitigating the diffusion limitations have focused on decreasing sizes to make nanocrystals (variation of gel/sol concentration and composition and modifiers)[15–19] and two-dimensional sheets/plates

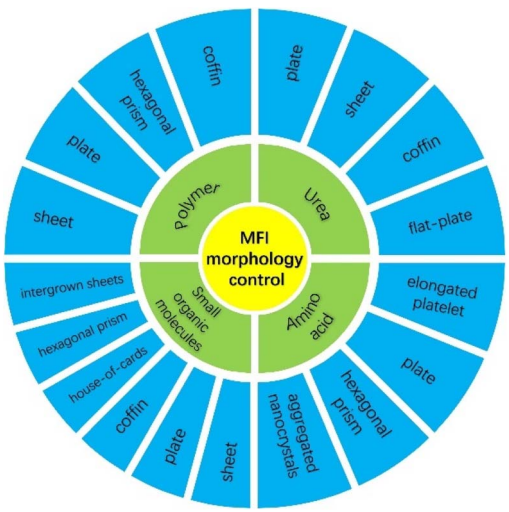

Scheme 1 Overview of MFI zeolite morphology control using different modifiers.

[a]*Key Laboratory of Marine Chemistry Theory and Technology, Ministry of Education, College of Chemistry and Chemical Engineering, Ocean University of China, Qingdao 266100, China. E-mail: feng.shao@ouc.edu.cn*

[b]*The ZeoMat Group, Qingdao Institute of Bioenergy and Bioprocess Technology, Chinese Academy of Sciences, Laoshan District, Qingdao 266101, China. E-mail: lupeng@qibebt.ac.cn*

[c]*Normandie University, ENSICAEN, UNICAEN, CNRS, Laboratoire Catalyse et Spectrochimie, F-14000 Caen, France. E-mail: valentin.valtchev@ensicaen.fr*

Table 1 Summary of MFI zeolites with different morphologies using modifiers

Additive type	OSDA type	Phase/product	Morphology	Preferred orientation/ thickness	Ref.
Urea only	TPAOH	ZSM-5	Sheet	*b*-Axis/90–110 nm	31
				b-Axis/80–100 nm	32
				b-Axis/0.12–0.33 μm	33
	TPABr	ZSM-5	Sheet	*c*-Axis/2.1 μm	34
	TPAOH	TS-1	Sheet	*b*-Axis/50 nm	35
	TPAOH	H-ZSM-5	Sheet	*b*-Axis/720–245 nm	36
	TPAOH	Silicalite-1	Plate or sheet	*b*-Axis/50 nm	37
	TPAOH	MFI	Sheet	*b*-Axis/50–100 nm	38
	TPAOH	ZSM-5	Plate	*c*-Axis/—	39
	TPAOH	TS-1	Flat-plate or sheet	*b*-Axis/100 nm	40
Urea & isopropyl alcohol (IPA)	TPAOH	TS-1	Sheet	*b*-Axis/80 nm	41
				b-Axis/95 nm	42
	TPAOH	ZSM-5	Sheet	*b*-Axis/100 nm	43
	TPAOH	H-ZSM-5	Plate	*b*-Axis/60 nm	44
	TPAOH	H-ZSM-5	Coffin	*b*-Axis/60–250 nm	45
Urea as alkalinity regulator	TPAOH	ZSM-5	Aggregated nanocrystals	*b*-Axis/∼160 nm	46
L-Carnitine & ethanol	TPAOH	TS-1	Elongated platelet	*b*-Axis/∼300 nm	47
D-Arginine	TPAOH	MFI	Elongated plate	*b*-Axis/—	48
L-Lysine	TPAOH	MFI	Hexagonal prism	*b*-Axis/∼56 nm, ∼37 nm	49
L-Glutamic acid	TPAOH	Silicalite-1	Nanocrystals	—/av. 60 nm	50
		TS-1		—/av. 100 nm	
L-Lysine	TPAOH	ZSM-5	Nanocrystals	—/∼100 nm	51
L-Lysine	TPAOH	Silicalite-1	Nanocrystals	—/50–450 nm	52
Diols (EG, DEG, TEG, and tEG)	TPAOH	Silicalite-1	Plate (hexagonal prism)	*b*-Axis/0.11–0.25 μm	53
Pyrocatechol	TPA^+	H-ZSM-5	Sheet	*c*-Axis/∼548–1530 nm	54
Ethanol	TPAOH	ZSM-5	Sheet	*b*-Axis/90 nm	55
Spermine	TPAOH	Silicalite-1	Platelet	*b*-Axis/<300 nm	56
Tributylphosphine oxide (TBPO)	TPAOH			*b*-Axis/<150 nm	
Triethylenetetramine (TETA)	TPAOH		Coffin	—/—	
Triethylamine	$C_{18-6-6}Br_2$	ZSM-5	Intertwined nanosheets; multilamellar nanosheets with house-of-cards	*b*-Axis/8–10 nm	57
N-Methyl-2-pyrrolidone	—	ZSM-5	House-of-cards	*b*-Axis/100 nm	58
Allophanamide	TPABr	ZSM-5	Sheet	*c*-Axis/—	34
Tetramethylguanidine (TMG)	TPAOH	ZSM-5	Plate	*b*-Axis/85 nm	59
Guanidine	TPAOH	ZSM-5, TS-1	Plate	*b*-Axis/75–110 nm	60
Imidazolium salts	TPABr	Silicalite-1	Coffin	*c*-Axis/5.8–22.9 μm	61
Glucose	TPAOH	ZSM-5	Large prismatic	—/—	62
				L_c = 3.5–5.0 μm	
	TPAOH	H-ZSM-5	Plate	*b*-Axis/300–500 nm	63
Propylene diamine Piperidine Catechol	TPABr	ZSM-5	Plate	—/—	64
Pyrrolidine Tetrahydrofuran	TPABr	ZSM-5	Sheet	*b*-Axis/90 nm	
Hexamethylenetetramine (H-amine)	TPAOH	ZSM-5	Noodle-like	*c*-Axis/—	39
				L_c/L_b = 35; L_a/L_b = 3	
Tributylphosphine oxide (TBPO)	TPAOH	MFI	Coffin (membrane)	*b*-Axis/1.1 ± 0.1 μm	65
Poly(hexamethylene biguanide) hydrochloride	TPAOH	MFI	Coffin (membrane)	*b*-Axis/∼400 nm	66
PEG2000	TPAOH	H-ZSM-5	Hexagonal prism	*b*-Axis/300–500 nm	67
Gelatin	TPABr	ZSM-5	Sheet	*b*-Axis/—	68
	TPAOH	TS-1	Plate	*b*-Axis/40–300 nm	69
Polyacrylamide	TPAOH	H-ZSM-5	Hexagonal prism	*c*-Axis/30 μm	70
			Elongated prism	*c*-Axis/40 μm	
Polyethylene oxide–polypropylene oxide–polyethylene oxide (P123)	TPAOH	TS-1	Stacked nanoplate	*b*-Axis/20–25 nm (unilamellar)	71

(organic structure-directing agents, OSDAs),[20,21] and generating mesopores through templates (surfactants)[22–25] or post-treatments (alkaline and acid etching).[26–28] A prominent breakthrough among those approaches was achieved by Ryoo *et al.*, who synthesized hierarchical MFI zeolites composed of unit-cell nanosheets with mesopores using pre-designed surfactant-based OSDAs.[29] Fluoride-mediated synthesis has been proven effective for obtaining two-dimensional MFI zeolite plates.[30] Although the surfactant and fluoride strategies are very promising from the academic point of view, their practical implication might be hindered considering the high cost and non-environmental friendliness. Thus, economic and eco-friendly methods are still needed for obtaining MFI zeolites with desired morphologies.

In this review, instead of providing a comprehensive overview of morphology manipulation methods, we focused on summarizing morphology control approaches of MFI zeolites using different organic modifiers, including urea, amino acids, small organic molecules, and polymers (Scheme 1). These modifiers have demonstrated capability to induce different morphologies, such as nanocrystals, nanosheets, plates, prisms, house-of-cards and intergrown sheets/plates. Importantly, these organic modifiers are cost-effective, considering industrial applications. The possible formation mechanisms of MFI zeolites with certain morphological features together with their advantageous applications are briefly summarized using specific additives. The perspectives and future challenges are also presented. A summary of MFI zeolites with various morphologies is given in Table 1, where the categorization is made based on the additive types, OSDA types, phases or products obtained, morphologies of the crystals and preferred orientation together with dimensions along the specific crystallographic axis.

2. Morphology control of MFI zeolites using organic additives

In recent years, great efforts have been made in enhancing the catalytic and separation properties based on the zeolite morphology control strategy. The current morphology control strategy mainly includes additive-assisted synthesis. Urea and amino acids are both classical morphology modifiers in the controllable synthesis of zeolites; thus in this work, we separate them from small organic molecules (Section 3), and review them as distinct categories on their own, respectively.

2.1 Urea

2.1.1 Urea only. Recently, Xiao's group synthesized ZSM-5 zeolite crystals with a shortened *b*-axis direction through a urea-assisted strategy.[32] ZSM-5 zeolite nanosheets (L_b = 80–100 nm, Si/Al = 21) were synthesized by crystallization at 180 °C for 2 days, using commercial tetrapropylammonium hydroxide (TPAOH) as the OSDA and urea as a growth inhibitor. By mixing ZSM-5 zeolite nanosheets with polyethylene raw materials in flowing hydrogen at 280 °C, short-chain olefins (C_1–C_7) were obtained with a yield of up to 74.6%, of which 83.9% were C_3–C_6 olefins, and there was almost no coking observed. In another study, they investigated the performance of Na–FeC_x (iron carbide catalyst)/zeolites for the low-temperature Fischer–Tropsch synthesis to olefins (LT-FTO) reaction.[31] The *b*-axis thickness of urea-assisted ZSM-5 zeolite nanosheets (s-ZSM-5) is 90–110 nm, while that of ordinary ZSM-5 zeolite (n-ZSM-5) is massive (Fig. 1A). The LT-FTO reaction in both zeolites shows an increase in the CO conversion rate, but the product selectivity is very different. Na–FeC_x/s-ZSM-5 achieves higher olefin selectivity, while Na–FeC_x/n-ZSM-5 shows high alkane selectivity. The reason is that the s-ZSM-5 zeolite indeed accelerates the desorption of olefins once they are formed on the Na–FeC_x surface *via* C–C coupling in the LT-FTO reaction, which is favourable for the continuous hydrogenation of CO. However, there is a serious diffusion limitation of olefins in the Na–FeC_x/n-ZSM-5 catalyst, making the hydrogenation of olefins to form alkane products easier (Fig. 1B).

Liu *et al.* synthesized sheet-like ZSM-5 zeolites with controllable *c*-axis length (called U-ZSM-5-*x*, where *x* = urea/silica) using tetrapropylammonium bromide (TPABr) as the OSDA and urea as the modifier by a one-pot solvent-free method.[34] SEM inspection revealed that compared with a urea-free zeolite (named SH-ZSM-5), the *c*-axis of the nanosheet synthesized using U-ZSM-5-0.03 is increased by about twice (from 1.2 μm to 2.1 μm), and the *b*-axis is reduced by about half (from 0.9 μm to 0.4 μm). The performance of methanol to gasoline (MTG) was evaluated. The methanol conversion rate was 100%, which was higher than that of ZSM-5 with conventional morphology, and the lifetime was up to 900 h.

Bao's group drew inspiration from previous urea-assisted methods for the preparation of sheet-like ZSM-5 crystals, aiming to improve their catalytic activity in syngas to aromatics (STA) reaction.[33] They investigated the optimal synthesis conditions for ZSM-5 nanosheets by adding different amounts of urea. The synthesis was performed using the gel molar

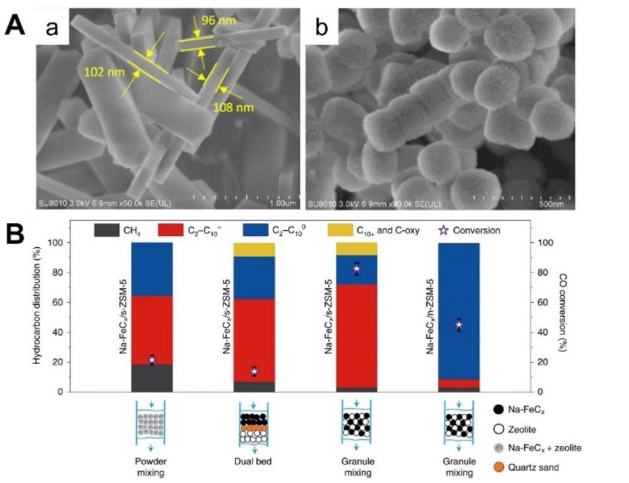

Fig. 1 (A) SEM images of (a) s-ZSM-5 and (b) n-ZSM-5. (B) Performance of catalysts, using different mixing methods, in the LT-FTO. Reprinted from ref. 31 with permission from Springer Nature Ltd, copyright 2022.

composition of $SiO_2 : Al_2O_3 : TPAOH : H_2O : urea = 1 : 0.0025 : 0.4 : 45 : x$, where $x = 0$–2.8, and the mixture was crystallized at 180 °C for 4 days. The XRD pattern shows that the zeolite sample with a urea/silica ratio of 2.8 exhibits a preferred orientation at $2\theta = 8.9°$, indicating that the sample has a sheet-like structure. When the urea/silica ratio is 0.5, the crystal has sheet-like morphology ($L_c = 1.58$ μm and $L_b = 0.12$ μm). Then, they continued to increase the amount of urea and found that the crystal size on each axis became larger. They performed the STA reaction over $ZnCrO_x$–ZSM-5, and found that a lower *b*/*a* axis length ratio of zeolites led to formation of more aromatics, but the selectivity of CH_4 and C_2–C_4 was not influenced.

Zhang *et al.* synthesized sheet-like TS-1 zeolite with a short *b*-axis at 170 °C by introducing urea as a growth inhibitor in the initial synthesis and adding seeds.[35] The *b*-axis thickness of the TS-1 zeolite prepared by pre-crystallization at the aging solution stage is as small as 50 nm. From SEM images, the TS-1 particles without urea and seed crystals are ellipsoidal (particle size over 500 nm). The morphology of the TS-1 synthesized by adding urea changed from an elliptical shape to a thin plate shape (*ca.* 250 nm), while the TS-1 synthesized by adding urea and seed crystals had a shorter *b*-axis (*ca.* 190 nm). Meanwhile, based on the synergistic synthesis of sheet-like TS-1 zeolite with urea and seed crystals, they also found that pre-crystallization at 80 °C can produce 50–60 nm thick sheet-like TS-1 zeolite. The performance of epoxidation of 1-hexene was evaluated between sheet-like TS-1 and conventional TS-1. The conversion rates of 1-hexene and the selectivity of 1,2-epoxyhexane were 48.2% *vs.* 50.7% and 80.4% *vs.* 33.5%, respectively.

Zhu *et al.* investigated the effects of adding urea and different aluminum source types in the initial gel on MFI-type zeolites and prepared HZSM-5 zeolites with different *b*-axis thicknesses and Si/Al ratios.[36] Herein, the initial aluminosilicate gel with molar composition of $1SiO_2/mAl_2O_3/0.12Na_2O/0.25TPAOH/100H_2O/n$urea ($m = 0.004$–0.01, $n = 0.6$, 1.0, 2.0) was crystallized at 150 °C. ZSM-5 zeolite with a *b*-axis thickness of 340 nm was synthesized when urea content was equal to 1.0. At the same time the crystallization mechanism of ZSM-5 zeolite after the addition of urea was studied. They found that during the crystallization process, the $-NH_2$ of urea interacts with the Si–OH on the surface of the crystal [010], significantly inhibiting the growth of ZSM-5 crystals in the *b*-axis direction (Fig. 2). The zeolite was then used for hexane cracking. The selectivity of light olefins was the highest (46.5%), which was 12.2% higher than that of the control sample under the same conditions due to lower C_B/C_L synergism and better mass transfer and diffusion properties.

Lv *et al.* synthesized Co@MFI zeolites with a controllable short *b*-axis and sheet thickness ranging from 50 nm to 130 nm with the assistance of urea.[37] The cobalt metal introduced *in situ* existed in the form of subnanometer CoO clusters with an average particle size of 0.88 nm. The *in situ* incorporation of cobalt did not affect the synthesis of the short *b*-axis morphology. The limited Co clusters in MFI zeolites have three kinds of pore placement, namely, in straight pore channels, sinusoidal pore channels and cross pore channels. The lowering

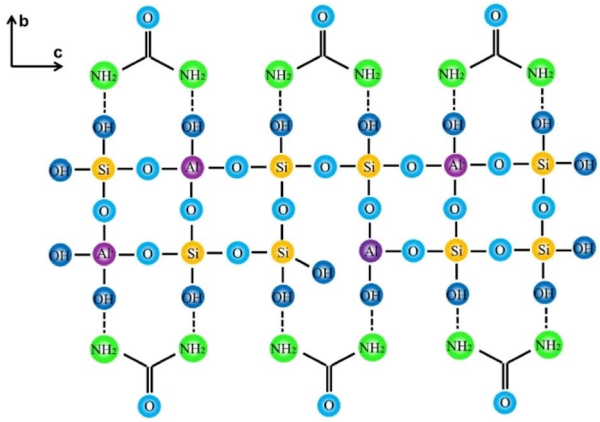

Fig. 2 Mode of action of urea in the *b*-axis direction. Reprinted from ref. 36 with permission from Elsevier Inc., copyright 2023.

of thickness increases the proportion of CoO subnano-clusters in straight pore channels by nearly two times. In addition, the acidic properties of the catalyst are also modulated, and the thinner the thickness, the stronger the Lewis acidity, and the stronger the ability to complex with NO probe molecules. When the three kinds of Co active sites catalyze propane dehydrogenation, Co in the straight pore channel has the lowest first step dehydrogenation heat. Therefore, we hypothesized that CoO subnano-clusters located in the straight pore channel are the best active sites for Co-based catalysts to catalyze propane dehydrogenation. Experimental results show that the catalyst with the thinnest *b*-axis thickness (denoted as Co@MFI-P50) has excellent propane activation ability. The initial conversion rate of propane was 41.8%, the highest propylene generation rate was 15 mmol C_3H_6 per g_{Co} per min, the propylene selectivity was 92%, and propane remained active after 9 regeneration cycles.

Recently, Mintova and co-workers reported the synthesis of plate-like MFI zeolites (silicalite-1 and ZSM-5) with controllable *b*-axis thickness ranging from 50–100 nm using urea as an additive.[38] They used TPAOH as the OSDA, the concentration of which, together with parameters like water and urea content, determined the growth behavior of MFI zeolites. The mechanistic study performed on pure silica MFI showed that urea could control the anisotropic growth at the early nucleation stage, generating rectangular crystals; then the growth along the *b*-axis can be suppressed to obtain plate-like morphology with synergistic effects of optimized synthesis parameters (Fig. 3). The introduction of Al in the synthesis of plate-like MFI showed that the increase in Al increased the crystal size. Besides, the choice of Si and Al sources could affect the morphology, *e.g.*, plate-like single crystals were obtained when TEOS and $Al(OH)_3$ were employed, whereas agglomerated or intergrown crystals formed when other silica sources were used.

2.1.2 Urea together with the second additive. Xiao's team first reported the use of urea combined with isopropanol in MFI zeolite morphology control.[41] They added urea into the initial titanosilicate gel with a molar composition of $SiO_2/0.02TBOT/0.3TPAOH/40H_2O/0.33$ isopropanol/0.074–0.368 urea, and

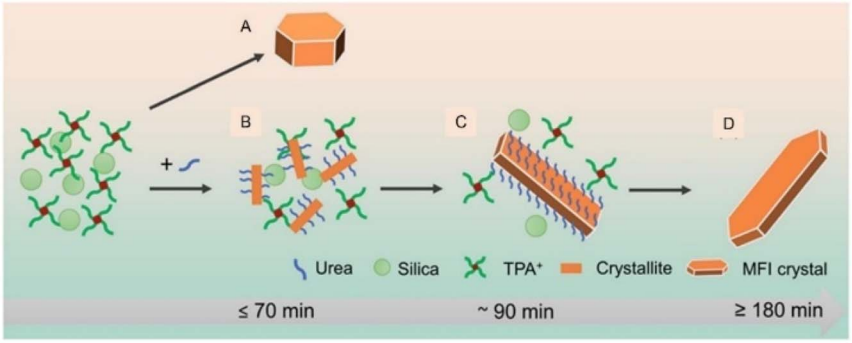

Fig. 3 Schematic representation of the MFI crystallization in the absence or presence of urea as an additive. Hexagonal prism crystals were obtained in the absence of urea (A). When the urea additive was added, rectangular crystallites were observed after about 1 hour (B), followed by the growth of nanosheet crystals with unfinished two ends (C), and finally coffin-shaped MFI nanosheets were formed (D). Reprinted from ref. 38 with permission from Springer Nature Ltd, copyright 2023.

crystallized it at 180 °C to prepare sheet-like TS-1 zeolite (TS-1-S) with a controllable *b*-axis length (Fig. 4). When urea/SiO_2 is equal to 0.368, the *b*-axis thickness of TS-1-S1 crystals is the smallest, *ca.* 80 nm, and L_a is *ca.* 400 nm. Later, they also synthesized ZSM-5 zeolites with controllable *b*-axis thickness *via* the initial gel composition of $1.0SiO_2/0.005Al_2O_3/0.3$TPAOH/$20H_2O$/(0.5–1.25) urea.[43] Compared with the gel system without the addition of urea, when the urea/SiO_2 is equal to 1.25, the synthesized sample is a uniformly sized single-piece zeolite, and the *b*-axis decreases from 200 nm to 100 nm. Wang and co-workers used urea as an additive and isopropyl alcohol to synthesize *b*-oriented H-ZSM-5 zeolites with different Si/Al ratios, and then studied the catalytic performance of different *b*-axis lengths and acidic samples in glycerol dehydration to acrolein (GDTA).[44] They synthesized H-ZSM-5 zeolites using the gel molar composition of $SiO_2 : Al_2O_3 :$ TPAOH : NaO : H_2O : urea : isopropanol = $0.053 : x : 0.016 : 0.0025 : 1 : 0.03 : 0.0016$ (x = 0.0044–0.00089) and found that the plate-like H-ZSM-5 zeolite (Si/Al = 75) with a *b*-axis thickness of about 60 nm achieved a high glycerol conversion (98%) and acrolein selectivity (87%) at a relatively high WHSV (4 h^{-1}). Later, they also synthesized *b*-oriented H-ZSM-5 zeolites (60, 130, 180 and 250 nm, Si/Al = 200) *via* the similar aluminosilicate gel composition and evaluated their performance on GDTA.[45] The results showed that H-ZSM-5 with a thickness of 60 nm had the highest acrolein selectivity up to 88%, ascribed to the higher microporous active site accessibility and shorter mass transfer channels in short *b*-axis MFI zeolites.

Xie's group aimed to investigate the effect of a few specific additives on the morphology of ZSM-5 zeolites by adding them to aluminosilicate gel and studied the mechanism of additive adsorption preferences on the anisotropic growth of ZSM-5.[39] ZSM-5 zeolites with different morphologies, such as sphere-like (butanone), plate-like (urea and pyrocatechol), and noodle-like (hexamethylenetetramine) were synthesized. Using TPAOH as the OSDA, ZSM-5 with added urea has a length-to-height ratio between 5 and 20 and an average width-to-height ratio of ~3, showing a two-dimensional plate-like structure, but its *b*-axis thickness is slightly greater. To understand the mechanism of the effect of additives on the anisotropic growth of ZSM-5 crystals, the authors conducted parallel controlled experiments and selected 8 typical additives to regulate the crystal morphology of ZSM-5 zeolites. The authors believe that there are two main reasons for the anisotropic growth of ZSM-5 zeolite: one is the adsorption preference of additives, and the other is the different crystallization kinetics.

Ping *et al.* added urea into the synthesis system to study the effect of urea addition on the morphology of MFI-type titanosilicate zeolite (TS-1), and further investigated its performance in propylene gas phase epoxidation to propylene oxide (PO).[42] They used commercial TPAOH as the OSDA, urea as a crystal growth regulator, and a small amount of isopropyl alcohol as an auxiliary to synthesize sheet-like titanium silicalite-1 zeolites (abbreviated as TS-1-S-x, x representing urea/SiO_2) at 170 °C. With the increase in urea content from 0.15 to 0.35, TS-1-S-0.35 (L_b = 95 nm) with a thinner *b*-axis thickness was obtained, indicating that urea significantly inhibited the growth of crystals along the *b*-axis. Finally, TS-1 loaded with Au (marked as Au/TS-1) was used to catalyze PO. Compared with TS-1 and TS-1-S-

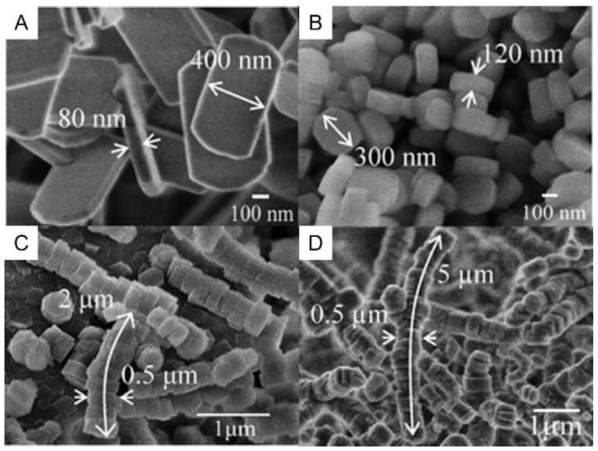

Fig. 4 SEM images of (A) TS-1-S1, (B) TS-1-S2, (C) TS-1-C1, and (D) TS-1-C2 samples. Reprinted from ref. 41 with permission from the Royal Society of Chemistry, copyright 2011.

0.35, TS-1-S-0.15 has the highest PO formation rates of 85 g_{PO} h^{-1} $kg_{cat.}^{-1}$ over 80 g_{PO} h^{-1} $kg_{cat.}^{-1}$ and 57 g_{PO} h^{-1} $kg_{cat.}^{-1}$. Although the short *b*-axis TS-1-S is favorable for mass transfer and diffusion, excessive urea is unfavorable for Ti incorporation into the zeolite framework, resulting in poorer performance of PO compared to TS-1 zeolite.

Later, Xu *et al.* also studied the catalytic performance of propylene epoxidation with H_2 and O_2 (HOPO process).[40] TS-1 zeolites with different amounts of urea were synthesized as supports. SEM analysis showed that when *x* was 0.15, the TS-1 morphology was elliptic. When *x* is increased to 0.30, TS-1 zeolite has a flat morphology with a *b*-axis length of about 100 nm. Then, they loaded Au onto the modified TS-1 zeolite (Au/TS-1) for HOPO to propylene oxide (PO). Compared with common ellipsoidal TS-1 zeolites with 200 nm and 500 nm crystal sizes, plate-like TS-1 zeolites have the highest PO formation rate (*ca.* 82 g_{PO} h^{-1} kg_{TS}^{-1}).

Interestingly, unlike the previous work on urea-assisted preparation of nanosheets, using urea as an additive, Ma *et al.* obtained a hierarchical mesoporous MFI-type ZSM-5 zeolite with an aggregated nanocrystalline structure through one-pot hydrothermal synthesis.[46] Compared with urea as a modifier to control the anisotropic growth of zeolites, urea here provides a mild, stable and homogeneous alkaline medium in the synthesis of hierarchical mesoporous zeolites. The alkalinity is provided by ammonia, which is the product of hydrolysis reaction of urea solution under controlled conditions. In addition, the crystallinity of zeolites treated with urea solution is perfectly preserved and mesoporosity can be successfully developed.

2.2 Amino acids

Watanabe *et al.* synthesized zeolites by adding an amino acid called L-glutamate (L-Glu) to the gel system.[50] Nano-sized all-silica MFI zeolite (silicalite-1) with an average particle size of 60 nm was synthesized with a gel molar ratio of 1.0TEOS/0.25TPAOH/0.016 L-Glu/11H_2O (Fig. 5A). Among them, L-Glu acts as a growth inhibitor to reduce the size of the crystal nucleus for obtaining nano-zeolite crystals. They also successfully synthesized titanosilicate zeolite (TS-1, av. 100 nm) by adding L-Glu (Fig. 5B). The epoxidation of cyclohexene with different sizes of TS-1 (100 nm, 190 nm and 305 nm) was carried out. The initial reaction rates of cyclohexene conversion were 3.0×10^{-3}. 1.2×10^{-3} and 9.8×10^{-4} mmol min^{-1}, respectively.

Deng *et al.* added L-lysine to the parent gel system to adjust the morphology of silicalite-1.[52] A series of silicalite-1 catalysts with a particle size between 50 and 450 nm were prepared by gel hydrothermal synthesis with a molar composition of 1.0TEOS/0.3TPAOH/*x* L-lysine/*y*H_2O. It was observed by SEM that crystal grains have smooth surfaces and uniform size. It is worth mentioning that by adding L-lysine, they significantly reduced the size of the silicalite-1 grains, and the nanoscale nucleus is favorable for the subsequent crystallization of thinner nanoparticles or nanoparticle zeolites. Herein, the synthesized nano-silicalite-1 and its NaOH-modified derivatives catalyzed the gas-phase Beckmann rearrangement of cyclohexanone oxime to caprolactam at WHSV = 6 h^{-1}, 370 °C. The results show that nano-silicalite-1 with the smallest particle size over cyclohexanone oxime conversion is nearly 100%, while the selectivity to ε-caprolactam reaches a maximum of 96.4%.

Yu's group obtained high-quality single-crystalline MFI-type nanozeolites (silicalite-1) with hexagonal prism morphology under the synergistic action of amino acids and multi-step crystallization.[49] Nanosized silicalite-1 (10–50 nm) was synthesized by two-step crystallization at 80 °C and 170 °C using a gel molar ratio of 1.0SiO_2/0.45TPAOH/*x* L-lysine/9H_2O (*x* = 0 and 0.1). The first step at low temperature (80 °C) is favorable for forming metastable irregular nanoparticles. Next, the temperature was raised to 170 °C, resulting in high-quality nanosized crystals with regular morphology. During the crystallization process, the growth inhibitor L-lysine causes metastable irregular nanoparticles to rearrange into morphology toward an equilibrium crystal shape (Fig. 6). They used a similar method to synthesize ZSM-5 zeolites to evaluate the performance in methanol to propylene (MTP) conversion, and found that the propylene selectivity was as high as 49% and the catalyst life was extended by 54 h. Subsequently, they used a L-carnitine-assisted

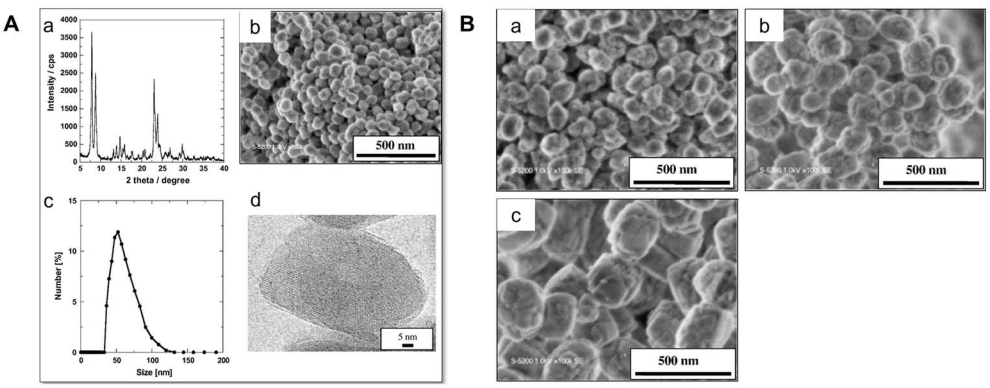

Fig. 5 (A) Synthesis of nanosized silicalite-1 with an av. size of 62 nm. (a) XRD pattern, (b) FE-SEM image, (c) DLS curve, and (d) HR-TEM image. (B) FE-SEM images of the TS-1 samples synthesized with the gel molar composition of 1.0 TEOS : 0.033 TBOT : 0.23 TPAOH : 0.016 L-Glu : *x* H_2O. (a) *x* =12, (b) *x* =18, and (c) *x* =32. Reprinted from ref. 50 with permission from Elsevier Inc., copyright 2011.

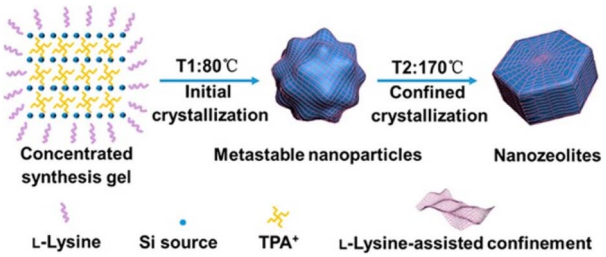

Fig. 6 Scheme for the proposed formation process of nanosized zeolites *via* synergetic use of the L-lysine-assisted approach and two-step crystallization in a concentrated gel system. Reprinted from ref. 49 with permission from American Chemical Society, copyright 2018.

one-step hydrothermal route to synthesize plate-like TS-1 zeolites with different coordinated Ti species, which were respectively denoted as TS-1#A_15Et:0.4LC (hexagonal plate, TiO_4) and TS-1#B_15Et:0.6LC (elongated platelet, TiO_6).[47] XRD shows that the TS-1#B_15Et:0.6LC and TS-1#C_0Et:0.6LC samples show a preferred orientation on the [020] crystal surface, which suggests the growth of plate-like zeolites. Meanwhile, SEM showed that L-carnitine/SiO_2 = 0.6 was the best addition amount (Fig. 7). Finally, they carried out the epoxidation of alkene (EOA) with synthetic TS-1 zeolite samples. TS-1#B_15Et:0.6LC has excellent catalytic activity with a turnover frequency of 131 h^{-1}, twice that of conventional TS-1 zeolites.

Peng *et al.* also synthesized ZSM-5 nano-zeolites with L-lysine to support MnO_x species and investigated the catalytic performance of the MnO_x/ZSM-5 catalyst in the oxidation of toluene.[51] The molar composition of gel is $1.0SiO_2/0.54TPAOH/0.017Al_2O_3/0.0017Na_2O/x$ L-lysine/$9H_2O$ ($x = 0$ and 0.2), in which L-lysine is used as a growth modifier, and small particles of ZSM-5 zeolite (named Z5-$L_{0.2}$) of 100 nm size are obtained. Z5-$L_{0.2}$ is more favorable for separating supported MnO_x than large-sized zeolites with a size of 500 nm. Meanwhile, due to the abundant oxygen vacancies and surface adsorbed oxygen of Z5-$L_{0.2}$, the temperatures at which the conversion of toluene reaches 90% (T_{90}) is 315 °C for MnO_x/Z5-L_0, while the T_{90} for MnO_x/Z5-$L_{0.2}$ is 276 °C.

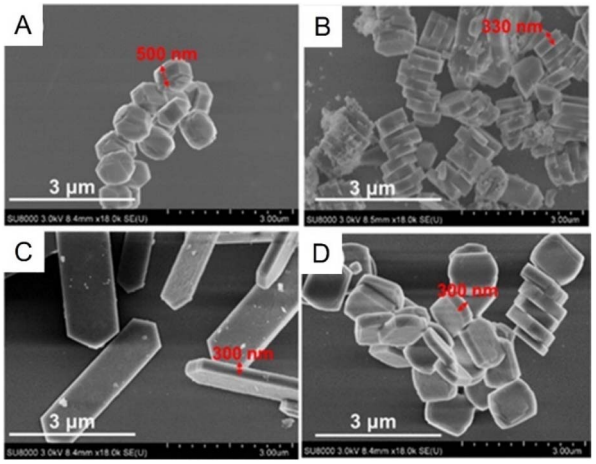

Fig. 7 SEM images of TS-1 zeolites assisted by L-carnitine. (A) TS-1#con, (B) TS-1#A_15Et:0.4LC, (C) TS-1#B_15Et:0.6LC, and (D) TS-1#C_0Et:0.6LC. Reprinted from ref. 47 with permission from American Chemical Society, copyright 2020.

Rimer and co-workers found that introducing D-arginine (D-Arg) into the gel could effectively control the anisotropic growth of silicalite-1 zeolites.[56] The addition of D-Arg results in a significant increase in the thickness of the *b*-axis of platelet-like silicalite-1 and a decrease in its length in the direction of the *c*-axis. This is due to the inhibitory effect of D-Arg on the growth of its [302] facet. This group investigated in depth the effect of D-Arg addition on the morphology of silicalite-1 zeolite[48] (Fig. 8). The addition of 0.3 wt% D-Arg to the gel increased the *b*-axis thickness of zeolites, so they concluded that D-Arg was more likely to bind to the [101] surface of silicalite-1 zeolites. Furthermore, they synthesized a series of hexagonal platelike zeolites by adding 0–7 wt% D-Arg. However, through crystal analysis and SEM, the crystal morphology was found to exhibit an unexpected changing trend. The *b*-axis thickness of the crystal increases with the increase in D-Arg concentration when the addition amount is 0–1 wt% D-Arg. In the range of 1–7 wt% D-Arg, the *b*-axis thickness of zeolite decreases monotonically with the increase in D-Arg concentration. Finally, they also proposed a crystallization mechanism for D-Arg, whereby D-Arg is decomposed *in situ* into ornithine lactam, which acts as a growth regulator to induce zeolite crystal size reduction, not through the traditional mechanism of preferentially binding crystal faces, but through its ability to hinder nanoparticle addition.

2.3 Small organic molecules

2.3.1 Small alcoholic molecules. Yu's group reported a new method for regulating the aspect ratio of silicalite-1 zeolite by adding diols combined with microwave heating.[53] Among them, diols including ethylene glycol (EG), diethylene glycol (DEG), triethylene glycol (TEG), and tetraethylene glycol (tEG) were used as co-solvents, and under microwave assisted heating, according to the initial gel composition of $1.0SiO_2$: 0.357TPAOH : 4EtOH : x diols : yH_2O, where x = 6–9, y = 21.55–45.55, the hexagonal prismatic plate-like silicalite-1 with *c*-axis orientation was synthesized. In addition, the type and concentration of diols also affect the *c*-axis length of silicalite-1 crystals. Finally, they proposed the kinetic mechanism of crystal growth of silicalite-1 zeolite under the action of diols as co-solvents. They suggested that this is related to adsorption theory, where the –O– groups of diols can form hydrogen bonds with local multi-Si–OH groups compared to monols. Under this strong force, the adjacent –CH_2–CH_2– groups come in close contact with the silicon species on the framework, thus further reducing the surface energy of the silicalite-1 crystals [010] and [100].

Xie's group synthesized H-ZSM-5 zeolites with short *b*-axis direct channels but different *c*-axis lengths by regulating zeolite morphology with the aid of pyrocatechol.[54] Herein, under alkaline conditions, H-ZSM-5 zeolites were prepared using the initial gel molar composition of $6TPA^+ : 20SiO_2 : 2.5Na_2O : 0.025Al_2O_3 : x$ pyrocatechol : 80EtOH : $800H_2O$, where x = 0–1.

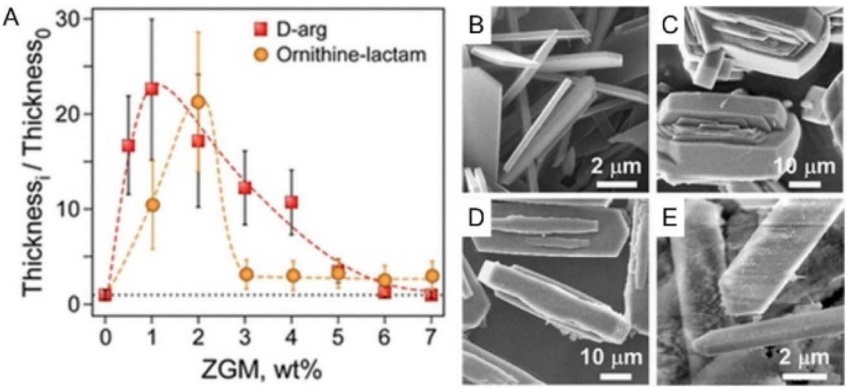

Fig. 8 Effect of the modifier on the morphology of silicalite-1 crystals synthesized from growth solution S(I). (A) Crystal thickness along the *b*-direction in the presence of D-Arg (red squares) or *R*/*S*-ornithine-lactam (orange circles) relative to the crystal thickness of the control, thickness$_0$, as a function of the modifier content. Each symbol is the average of more than 50 measurements from a single batch. Dashed lines are interpolated to help guide the eye, and error bars represent two standard deviations. (B–E) Scanning electron micrographs of silicalite-1 crystals prepared with the following synthesis conditions: (B) control (absence of the modifier), (C) 1, (D) 3, and (E) 7 wt% D-Arg. Solution S(I) : 40SiO_2 : 40TPAOH : 9420H_2O : 160EtOH. Reprinted from ref. 48 with permission from American Chemical Society, copyright 2019.

The SEM images showed that the *a*-axis and *b*-axis lengths of the synthesized H-ZSM-5 samples were about 250 nm and 100 nm, respectively, but only the *c*-axis length varied with the amount of pyrocatechol added (Fig. 9).

Zhu *et al.* constructed sheet-like ZSM-5 (marked as S-ZSM-5) zeolites with a controllable aspect ratio only by using an ethanol (EtOH) assisted strategy.[55] Herein, they systematically investigated various parameters (the kind of alcohol and the content of ethanol and H_2O) to screen out the optimal synthesis conditions for two-dimensional S-ZSM-5 zeolites, and synthesized S-ZSM-5 zeolites with a *b*-axis thickness of 90 nm and different aspect ratios. They also proposed the mechanism by which EtOH assisted in regulating the morphology of ZSM-5 zeolites. They suppose that EtOH containing –OH groups may preferentially interact with the exposed Si–OH group on the crystal [010] facets, inhibiting the growth along the *b*-axis and easily forming zeolites with a sheet-like morphology (Fig. 10). Because of its short straight channel and optimized acidity, S-ZSM-5 exhibits higher benzene conversion (*ca.* 8.5%) compared to conventional benzene-ring-like ZSM-5 (C-ZSM-5) (*ca.* 3.8%), and slightly higher ethylbenzene selectivity (*ca.* 95% *vs. ca.* 93%) in the alkylation of benzene with ethanol.

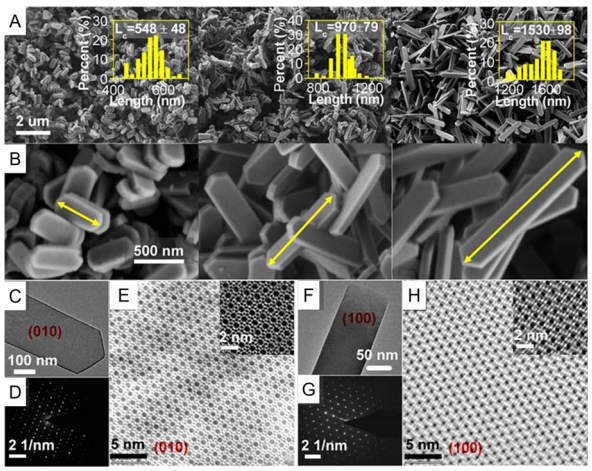

Fig. 9 The morphology of the as-synthesized H-ZSM-5 zeolites assisted by pyrocatechol. (A and B) SEM results of H-ZSM-5 zeolites with similar thicknesses of *a*- and *b*-axis but different lengths of *c*-axis. Left: Z-cS; middle: Z-cM; right: Z-cL. (C) TEM image of Z-cL sample with exposed facets of [010] plane. (D) The corresponding SAED patterns of [010] plane. (E) Aberration-corrected STEM image of Z-cL sample with exposed facets of [010] plane, with the inset on the top right displaying the STEM image with high resolution and the framework structure of H-ZSM-5 projected along [010] plane. (F–H) TEM image, the corresponding SAED patterns, and the aberration-corrected STEM image of Z-cL sample with exposed facets of [100] plane. Reprinted from ref. 54 with permission from Springer Nature Ltd, copyright 2021.

2.3.2 N-containing organics. Rimer's group found that various nitrogen-containing organic compounds are effective modifiers for controlling the anisotropic growth rate of silicalite-1 zeolites.[56] The selected modifiers are spermine ($C_{10}H_{26}N_4$), triethylenetetramine (TETA, $C_6H_{18}N_4$), and tributylphosphine oxide (TBPO). The experimental results showed that the addition of TBPO and spermine inhibited the growth of silicalite-1 zeolite along the *b*-axis, and micron-sized platelet-like silicalite-1 was prepared with crystal thicknesses of less than 150 nm and 300 nm, respectively. TETA, by contrast, is much less effective in regulating the thickness of silicalite-1 crystals. Finally, they proposed the theory of crystal surface adsorption, which states that specific functional groups in the modifier can bind to silicalite-1 specific crystal facets, thereby preventing the OSDA from guiding grain growth on that crystal facet (Fig. 11).

Wang *et al.* synthesized nanosheet-stacked hierarchical ZSM-5 zeolite with the assistance of triethylamine (TEA) as a modifier combined with crystal seeds.[57] Herein, they used the di-quaternary ammonium cation $[C_{18}H_{37}–N^+(CH_3)_2C_6H_{12}–N^+(CH_3)_2–C_6H_{12}]Br_2$ (abbreviated as $C_{18-6-6}Br_2$) as the OSDA,

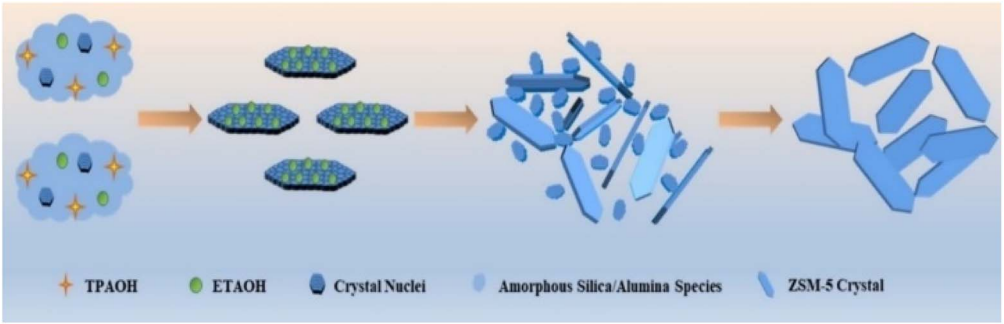

Fig. 10 Illustration of the formation of the sheet-like ZSM-5 zeolite with ethanol as an additive. Reprinted from ref. 55 with permission from Wiley-VCH GmbH, copyright 2023.

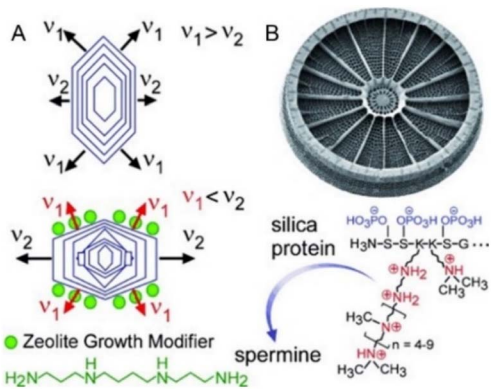

Fig. 11 (A) Native crystal habit (top) can be modified (bottom) by using molecules that bind to specific surfaces and alter anisotropic growth. (B) The amorphous silica exoskeletons of diatoms are formed through interactions with amine-rich proteins, which we mimic in silicalite-1 synthesis by using synthetic ZGM analogues. Reprinted from ref. 56 with permission from Wiley-VCH Verlag GmbH & Co. KGaA, Weinheim, Germany, copyright 2012.

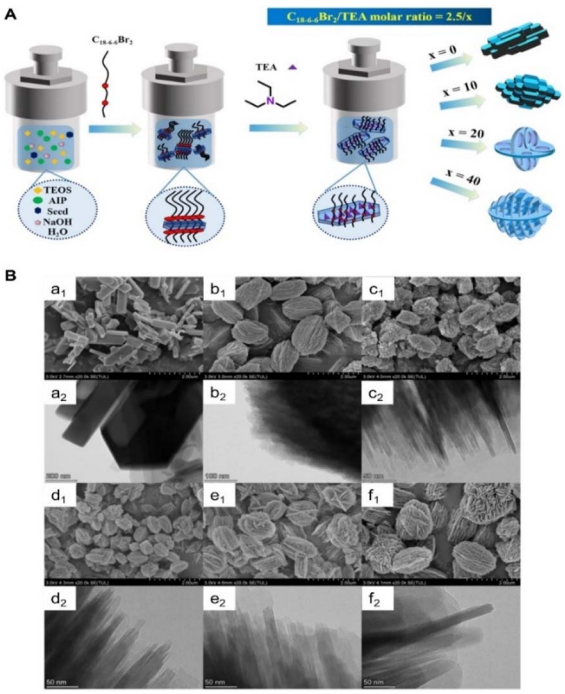

Fig. 12 (A) Graphical illustration of the formation of hierarchical ZSM-5 nanosheets during hydrothermal crystallization with different amounts of triethylamine addition. (B) SEM and TEM images of the ZSM-5 zeolite samples upon adding triethylamine. (a_1 and a_2) HZ5-0/0, (b_1 and b_2) HZ5-2.5/0, (c_1 and c_2) HZ5-2.5/5, (d_1 and d_2) HZ5-2.5/10, (e_1 and e_2) HZ5-2.5/20, and (f_1 and f_2) HZ5-2.5/40. Reprinted from ref. 57 with permission from MDPI, copyright 2022.

and studied the influence of TEA on the formation and morphology of ZSM-5 zeolites according to the mother gel molar composition of $7.5Na_2O/1Al_2O_3/125SiO_2/2.5C_{18-6-6}Br_2/4000H_2O/x$TEA (where, $x = 0$–40). When the molar addition of TEA increased from 5 to 40, the SEM images showed that the morphologies of ZSM-5 zeolites gradually transformed from monolayer platelet-like ZSM-5 zeolites with a small aspect ratio to a multilayer ZSM-5 stacked with nanosheets (Fig. 12). It is worth noting that the thickness of nanosheets is very thin, about 8–10 nm. Due to the easy access to acid sites and the hierarchical pore structure of nanosheet-stacked hierarchical ZSM-5 zeolites, they exhibit excellent catalytic activity and stability in catalyzing *n*-octane to light olefins, with a selectivity of 70.7%, representing an increase of 6.6% compared to conventional spherical ZSM-5.

Liu *et al.* constructed a new pathway for synthesizing house-of-cards-like ZSM-5 (abbreviated as HCL-ZSM-5) in the zeolite synthesis system without the addition of the OSDA, using a *N*-methyl-2-pyrrolidone (NMP) assisted strategy.[58] Based on the parent gel molar composition of $0.2Na_2O : 0.025Al_2O_3 : SiO_2 : 17.8H_2O : 0.808$NMP, the ZSM-5 obtained after crystallization at 140 °C for 48 h has higher crystallinity and is the pure MFI phase. Meanwhile, the SEM images show that the ZSM-5 zeolite is composed of intergrown sheets with a single sheet thickness of 100 nm (Fig. 13). HCL-ZSM-5 synthesized with the assistance of NMP has two advantages: firstly, it has a larger outer surface, and secondly, it has stronger acidic sites. Compared to conventional zeolite catalysts, HCL-ZSM-5 has the highest 1,3,5-triisopropylbenzene (TIPB) conversion of 90.5%, compared to 15.7% for ZSM-5, 21.3% for Y and 41.8% for Al-MCM-41.

Liu *et al.* synthesized *c*-axis oriented ZSM-5 zeolites with the assistance of allophanamide, an organic compound similar to

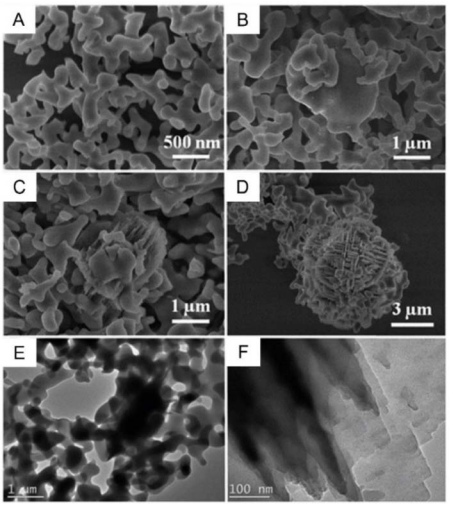

Fig. 13 SEM images of the products synthesized by introducing *N*-methyl-2-pyrrolidone at 140 °C for (A) 6 h, (B) 18 h, (C) 24 h and (D) 48 h. (E and F) TEM images of the products prepared by introducing *N*-methyl-2-pyrrolidone at 140 °C for 18 h and 24 h, respectively. Reprinted from ref. 58 with permission from RSC Publishing Group, copyright 2014.

urea, by a one-pot solvent-free method.[34] They used TPABr as the OSDA and added an organic amine (allophanamide) to the initial gel to obtain *c*-axis oriented sheet-like ZSM-5 zeolites. Allophanamide has a similar action mechanism to urea, and can be decomposed into NH_3 adsorbed on certain crystal facets at experimental temperatures. The sheet-like ZSM-5 catalyst for methanol to gasoline (MTG) achieves a methanol conversion of 100%, a high C_5^+ selectivity of 63.8%, and an extremely long lifetime of up to 900 h.

Shi's group reported the use of nitrogen-rich tetramethylguanidine (TMG) to assist the synthesis of short *b*-axis oriented ZSM-5 zeolites.[59] With an initial gel molar composition of $1.0SiO_2/0.01Al_2O_3/0.45TPAOH/18H_2O/x$TMG ($x = 0.2$, 0.3, 0.5, 0.7 and 0.9), plate-like ZSM-5 samples (abbreviated as P-ZSM-5-*x*) were hydrothermally synthesized by two-stage crystallization at 80 °C and 170 °C (Fig. 14). The SEM images show that P-ZSM-5-0.3 has crystal sizes of 290 × 85 × 840 nm ($a \times b \times c$). Finally, they put forward the mechanism of TMG, and believed that the existence of TMG transformed the initial gel into a colloid, and the colloidal particles attached to the crystal surface mainly along the *a*- and *c*-axis through the solid phase transition pathway. Later, this group selected more guanidine compounds, including tetramethylguanidine (TMG), dodecylguanidine hydrochloride (DGH), and polyhexamethylene biguanide hydrochloride (PHMB).[60] Plate-like MFI zeolites (silicalite-1, ZSM-5 and TS-1) with *b*-axis thicknesses of 75–110 nm were also obtained *via* a similar gel composition. Among the three guanidine compounds, the addition of DGH and PHMB appeared to effectively control the crystal growth compared to TMG. During the synthesis of ZSM-5 or TS-1 zeolites, more heteroatoms (Al or Ti) can enter the framework due to the action of organic guanidine modifiers.

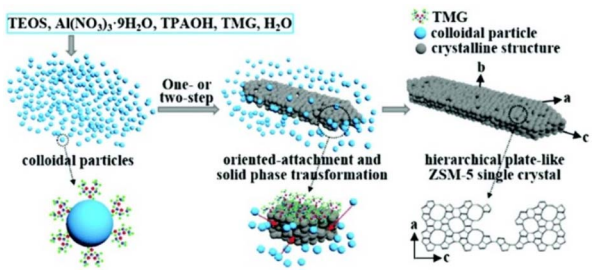

Fig. 14 Formation mechanism of single-crystalline hierarchical plate-like ZSM-5 crystals for zeolite syntheses in one step (at 170 °C) or in two steps (at 80 °C and then at 170 °C). Reprinted from ref. 59 with permission from the Royal Society of Chemistry, copyright 2022.

Rong *et al.*[61] investigated the effect of imidazole based ionic liquids on the morphology control of MFI zeolites by changing the type and dosage of imidazole based ionic liquids, which include 1-butyl-3-methylimidazole bromide ([C_4MIm]Br), 1-octyl-3-methylimidazole bromide ([C_8MIm]Br), 1-dodecyl-3-methylimidazole bromide ([C_{12}MIm]Br), and 1-hexadecyl-3-methylimidazole bromide ([C_{16}MIm]Br). The SEM images show that increasing the alkyl chain length or concentration (3, 5, 7.5 and 10 mmol) of imidazolium ionic liquids can result in small sized *c*-axis-oriented coffin-like silicalite-1 zeolites, indicating that the anisotropic growth of zeolites is affected by spatial steric hindrance.

2.3.3 Sugar molecules. Feng *et al.* used glucose-assisted methods to regulate the structure, acidity, and morphology of ZSM-5 crystals.[62] Glucose-modified ZSM-5 zeolites (named ZSM-5-T*x*, where T indicates two-stage hydrothermal crystallization and $x = 0$–4 indicates glucose/SiO_2 molar ratios of 0, 0.2, 0.3, 0.4, and 0.5, respectively) were hydrothermally synthesized with the gel molar composition of $1.0Al_2O_3 : 50SiO_2 : 2.0Na_2O : 8TPAOH : 3000H_2O : j$ glucose (where $j = 0$, 10, 15, 20, 25). SEM images show that ZSM-5-T3, with the optimal addition of glucose, displayed a large prismatic morphology (L_c = 3.5–5 μm). The methanol to propylene (MTP) reaction was carried out at 450 °C and a methanol WHSV of 3.8 h^{-1}, and ZSM-5-T3 exhibited the highest propylene selectivity up to 45.2%, a propylene/ethylene ratio of 8.4 and a $C_2^=$–$C_4^=$ selectivity of 63.9%. Later, Feng and co-workers again synthesized *b*-axis oriented nanosized H-ZSM-5 zeolites (L_b = 300–500 nm) *via* a similar gel molar composition of $50SiO_2 : 1.0Al_2O_3 : 8TPAOH : 12$ glucose $: 3000H_2O : n NH_4OH$ ($n = 10$, 20, 30, 50, 75, 100, and 125), with enhanced performance in the MTP reaction.[63] The obtained samples were abbreviated as Z5-G(1–7) corresponding to the values of *n*. In particular, the Z5-G3 catalyst presents the best catalytic performance (a high propylene selectivity of 50.98%, the highest light olefin selectivity of 79.46%, and the longest catalytic lifetime of 24 h).

2.3.4 Organic acids. Zhang *et al.* used organic weak acids/multicarboxylic acids (citric acid and nitrilotriacetic acid) as crystal morphologic modifiers to obtain plate-like titanium silicalite-1 (TS-1) zeolites.[72] With the gel molar composition of $1.0SiO_2 : 0.025TiO_2 : 0.36TPAOH : 0.1KOH : 0.15$ citric acid/nitrilotriacetic acid $: 35H_2O$, TS-1 zeolites were obtained by crystallization at 170 °C. Among them, TS-1 was marked as TS-1-

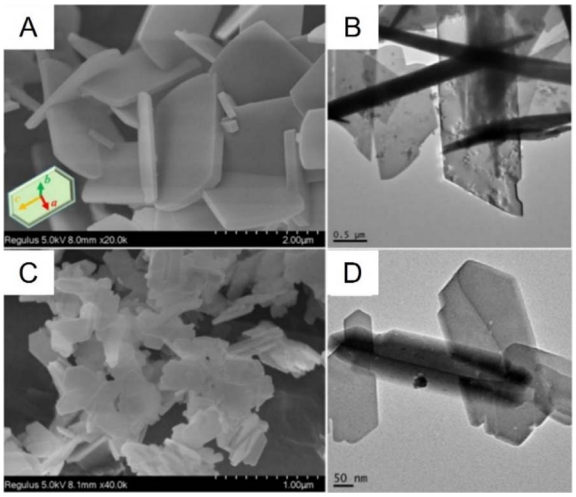

Fig. 15 SEM and TEM images of the calcined plate-like TS-1 product with the assistance of additives. (A and B) TS-1-CA and (C and D) TS-1-NTA. Reprinted from ref. 72 with permission from Elsevier B.V., copyright 2022.

CA for citric acid addition, with a crystal size of 1.5 × 0.2 × 2.0 μm ($a \times b \times c$) and TS-1-NTA (0.3 × 0.06 × 0.6 μm) for nitilotriotropic acid addition, respectively (Fig. 15). The XRD patterns show that TS-1 zeolites synthesized with the aid of polycarboxylic acid are pure MFI phase; the peak strength of TS-1 zeolite regulated by citric acid at the [020] crystal surface is higher than that at the [101] crystal surface, indicating a preferred orientation, which implies that TS-1-CA is a lamellar zeolite. TS-1-CA and TS-1-NTA both have large aspect ratios (L_c/L_b) greater than 10, which is one of the largest aspect ratios reported for TS-1 zeolites. The plate-like TS-1 modified with organic weak acids was used for 1-hexene epoxidation, showing higher conversion rates of 20.9% and 20.2%, and turnover numbers of 104 and 100 compared to conventional nano-sized TS-1, respectively.

2.3.5 Other small organic molecules. Xie's group screened more than thirty kinds of additives and found that the addition of propylene diamine, pethidine, and catechol to the initial gel was helpful in synthesizing platelike ZSM-5 zeolites, while more ideal sheet-like ZSM-5 zeolites were obtained by tetrahydrofuran modification.[64] From this, it can be concluded that adding special modifiers can effectively reduce the thickness of the *b*-axis of ZSM-5 zeolite crystals. They proposed that the formation of two-dimensional ZSM-5 zeolites is due to changes in crystal surface energy induced by introducing molecules with appropriate functional groups and polarity. Then, the synthesized ZSM-5 zeolites with different morphologies were used in the cracking reaction of C_4 olefins. The results indicate that 2D ZSM-5 zeolites with short *b*-axis orientation exhibit high catalytic performance, thereby verifying that zeolites with short *b*-axis orientation are beneficial for mass transfer and diffusion. Later, this group selected eight typical additives again to study their effects on the anisotropic growth of ZSM-5 zeolite crystals.[39] Following the gel molar ratio of $8TPAOH/20SiO_2/0.025Al_2O_3/(0–1)R/80EtOH/800H_2O$ (where, R represents different additives), ZSM-5 zeolites modified with different additives were obtained. Surprisingly, hexamethylenetetramine (H-amine)-modified ZSM-5 zeolite exhibits a typical noodle-like morphology ($L_c/L_b = 35$ and $L_a/L_b = 3$), whereas the plate-like ZSM-5 zeolite regulated by pyrocatechol has a slightly smaller aspect ratio ($L_c/L_b = 5–20$ and $L_a/L_b = 3$). The use of these two additives is beneficial for the growth of ZSM-5 zeolites along the *c*-axis direction. They believe that there are two main reasons for the anisotropic growth of ZSM-5 zeolites: first, the adsorption preference of additives inhibits or promotes the crystallization process, and second, there are differences in crystallization kinetics.

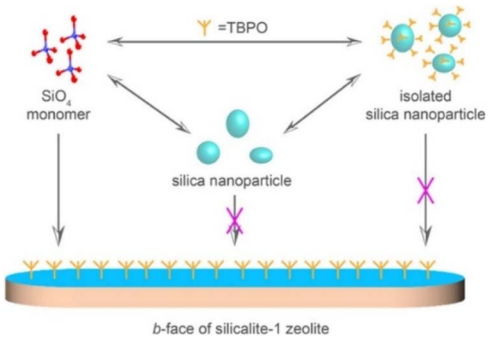

Fig. 16 Illustration of the role of TBPO in MFI crystal nucleation and growth. Synthesis condition: $1TEOS/0.2TPAOH/110H_2O$ at 150 °C. Reprinted from ref. 65 with permission from American Chemical Society, copyright 2018.

Wang *et al.* proposed to recover Xe from exhaled gas (CO_2/Xe) using a high-flux *b*-oriented MFI zeolite membrane of silica-coated alumina supports[65] (Fig. 16). They used commercial TPAOH as the OSDA and added 0–0.5 wt% tributylphosphine oxide (TBPO) as a morphology modifier. Under the action of TBPO, the *b*-face dimension of MFI zeolite membranes significantly increased, while promoting the secondary membrane-forming of coffin-like crystal seeds. The *b*-axis length of the monolayer of the MFI zeolite membrane remained around 350 nm when prepared with the assistance of TBPO. The prepared *b*-oriented MFI zeolite membranes exhibited a CO_2 permeance of 1213, which is several orders of magnitude higher than that of carbon molecular sieving membranes and polymeric membranes.

2.4 Polymers

Lv *et al.* used polymer-assisted synthesis for hierarchical TS-1 zeolite stacked 2D-nanoplates with constrained mesopores earlier.[71] They used commercial TPAOH as the OSDA and utilized polyethylene oxides–polypropylene oxides–polyethylene oxide (P123) lamellar micelles through a self-assembly process combined with multi-step crystallization to obtain lamellar nanoplate-like TS-1 zeolite. Among them, P123 plays two roles in the system: first, as a template for mesoporous TS-1 zeolite and the second as a morphology modifier for platelike TS-1 zeolites. The SEM images show that the total thickness of TS-1 zeolite stacked nanoplates is 100–120 nm, while the thickness of single-layer nanoplates is 20–25 nm (Fig. 17). The

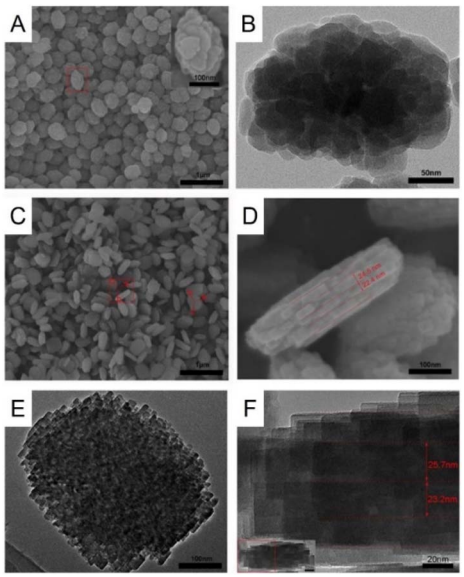

Fig. 17 SEM images and high-magnification SEM image of hierarchical TS-1 particles in the inset (A), TEM image of hierarchical TS-1 zeolite (B), SEM image of hierarchical TS-1 nanoplates (C), high magnification SEM image of hierarchical TS-1 nanoplates (D), and TEM image of hierarchical TS-1 nanoplates (E and F). Reprinted from ref. 71 with permission from Elsevier B.V., copyright 2018.

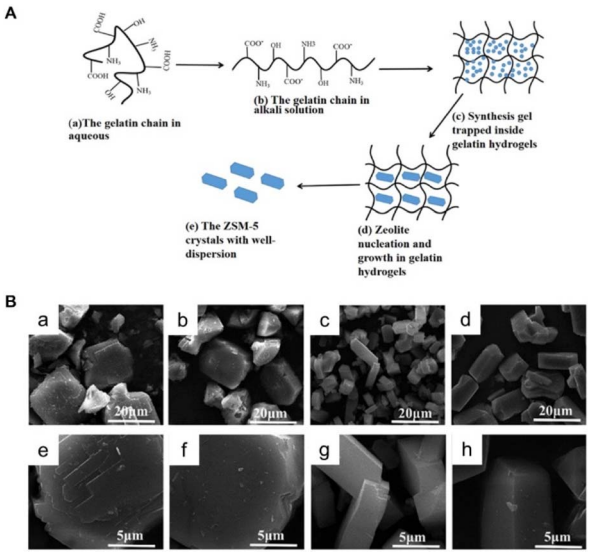

Fig. 18 (A) Schematic representation of the synthesis of ZSM-5 zeolite by using gelatin hydrogels. (B) SEM images of the ZSM-5 crystals obtained in the reaction systems with different mass ratios of gelatin/H_2O. (a and e) Gelatin/H_2O = 0 : 100; (b and f) gelatin/H_2O = 1 : 100; (c and g) gelatin/H_2O = 2 : 100; (d and h) gelatin/H_2O = 4 : 100. Reprinted from ref. 68 with permission from Taylor & Francis, copyright 2019.

oxidative desulfurization (ODS) performance of TS-1 zeolites with hierarchical pores was evaluated. TS-1 zeolite with hierarchically stacked nanoplates significantly shortened the time of a total oxidation of dibenzothiophene (DBT) within 40 min compared to the oxidation of DBT is 99.8% for 2 h of oxidation when using hierarchical TS-1 zeolite as the catalyst.

Chen *et al.* synthesized well-dispersed ZSM-5 zeolite with the aid of natural polymer gelatin.[68] Gelatin–H_2O mixture solutions with different mass ratios (gelatin/H_2O = 0–0.04) were prepared first, and then reagents such as OSDA, silicon source and aluminum source were dissolved in the solution, and the initial gel with a molar composition of $100SiO_2/Al_2O_3/8.5Na_2O/12TPABr/2500H_2O$ was obtained by hydrolysis overnight. After static crystallization at 180 °C for 48 h, ZSM-5 zeolites were obtained. When gelatin/H_2O is equal to 2 wt%, the morphology of ZSM-5 zeolite exhibits hexagonal sheets with the thinnest *b*-axis thickness (Fig. 18). Using the zeolite for catalyzing the conversion of methanol to hydrocarbons (MTH), the catalyst shows the longest lifetime of 95 h, with a selectivity of 28.5% for propylene, which is significantly better than that of ZSM-5 zeolite without the gelatin modifier. Later, Guo's group also used gelatin (GE) as a modifier to obtain TS-1 nanoplates with a *b*-axis thickness of 40–300 nm.[69] The SEM images show that when $m(GE/SiO_2)$ increases to 1.5, the obtained zeolites changed from nano aggregates to smooth sheet-like crystals (L_b = 40 nm). They also analyzed the working mechanism of gelatin on TS-1 nanoplates, and concluded that the synergistic action of amino and carboxyl groups in gelatin led to the morphological changes of TS-1 zeolites.

Guo *et al.* prepared *c*-axis-oriented HZSM-5 zeolites by the crosslinked polyacrylamide (C-PAM) hydrogel-assisted method.[70] By adding *in situ* synthesized C-PAM (0–2%) to the aluminosilicate gel, ZSM-5 zeolite grows directionally along the *c*-axis. SEM images show that the hexagonal prism-like ZSM-5 (called Z-2) containing 2% C-PAM gel has a large aspect ratio (L_c/L_b) (Fig. 19). The NH_3-TPD characterization results indicate that Z-2 has the strongest acidity, with a strong acid content of 0.163 mmol g^{-1}. Z-2 was used for the methanol to olefin (MTO) reaction, and it demonstrated complete methanol conversion, higher light olefin selectivity (81.2%), and the longest lifetime of over 23 h.

Zhou *et al.* synthesized hierarchical lamellar H-ZSM-5 zeolite (marked as HLHZ) through the one-step hydrothermal synthesis strategy assisted by water-soluble polymer polyethylene glycol (PEG2000).[67] A series of short *b*-axis HLHZ with hexagonal prism shapes were obtained using the gel molar ratio of $50SiO_2/$

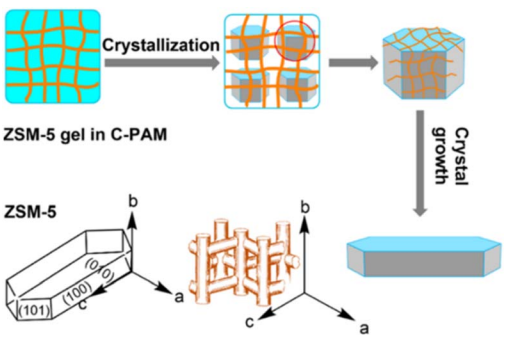

Fig. 19 Schematic representation of HZSM-5 zeolites directly synthesized in crosslinked polyacrylamide (C-PAM) hydrogels. Reprinted from ref. 70 with permission from Springer Science Business Media, LLC part of Springer Nature, copyright 2020.

$1.0Al_2O_3/10TPAOH/1500H_2O/1.0PEG2000/x$ urea (x = 20, 40, 60 and 80). The NH_4^+ from urea decomposition could balance the negative charge of the zeolite framework. PEG2000 serves as the template for ZSM-5 zeolite with a hierarchical pore structure, and also acts as a modifier to inhibit growth along the *b*-axis, shortening the *b*-axis length from 1 μm to about 300–500 nm.

Yang *et al.* introduced the modifier poly(hexamethylene biguanide) hydrochloride to fabricate highly *b*-oriented MFI zeolite (abbreviated as BOMZ) membranes on porous Al_2O_3 support during the secondary growth of crystal seeds.[66] When the ratio of initial gel is $1.0TEOS/0.2TPAOH/200H_2O/0.008PHMB$, the effect of inhibiting twin growth is the best. In addition, they also conducted in-depth research on the growth mechanism of BOMZ membranes in the presence of PHMB, and concluded that the introduction of PHMB regulates the crystallization kinetics by controlling the pH value of the synthesis system and preferential adsorption of the amino groups on the [010] surface of MFI crystals. The 650 nm thick BOMZ membrane prepared on a porous Al_2O_3 carrier exhibited excellent separation performance in the pervaporation of a 5 wt% $EtOH/H_2O$ solution at 60 °C, achieving a separation coefficient of 71 and a flux of 2.8 kg m^{-2} h^{-1}.

3. Effect of zeolite morphology on the catalytic performance

Two-dimensional zeolites (nanosheets, plates, intergrown nanosheets, intergrown plates, *etc.*) are characterized by their open framework structure, large external surface area, optimized surface acidity, easy access to active sites, and short diffusion path lengths, which endow it with excellent catalytic performance in reactions such as conversion of methanol, cracking, carbonylation, isomerization, alkylation, acylation and oxidation. Except for the spatial confinement effect, the metal dispersion and stability of the catalysts were also significantly affected by the interaction between the metal species and zeolite supports. Two-dimensional zeolites can effectively fulfill the requirements of an optimal support ascribed to their large external surface area and the presence of rich silanol defects. In particular, the abundant silanol groups in two-dimensional zeolites can effectively anchor the metal species, which can enhance the interaction between the metal and the support *via* the formation of strong covalent metal–oxygen bonds, and significantly improve the confinement effect and dispersion of the metal species in the interlayers and pores, thus forming and stabilizing the ultrasmall metal species, and thus improving the metal utilization. In addition, two-dimensional MFI zeolites possess a short *b*-axis direction, which is favorable for the rapid diffusion of molecules, avoiding deep reactions.

While the composition and pore structure of zeolites are essential, the particle size also significantly influences their properties and thus the performance in many chemical processes such as catalysis and separation. Low-dimensional zeolites such as "nanozeolites" (<100 nm) can improve reactivity and accelerate kinetics due to the much larger external surface area and shorter diffusion pathways. For instance, the gas-phase Beckmann rearrangement of cyclohexanone oxime to caprolactam[52] and methanol to propylene (MTP)[49] reactions were significantly improved by reducing the particle size of zeolites from the micro- to the nano-scale.

Therefore, based on a comprehensive review, it is not difficult to find that zeolite morphology has a significant effect on catalytic and separation performance upon comparison.

Finally, there are still important aspects to consider when choosing additives for the target morphology of zeolites, such as:

(1) First, the catalytic reaction itself should be considered (reactants/products and the reaction process) so that the ideal support morphology can be identified and then the morphology control can be performed purposefully.

(2) The principle of controlled synthesis of two-dimensional zeolites is to utilize the adsorption preference of additives to the crystal surface to influence the growth of a certain crystal surface. Consideration can be given to the choice of organic molecules containing $-NH_2$ and –OH groups as well as inorganic compounds (carbonates and nitrates).

(3) For the synthesis of low-dimensional zeolites such as nanocrystals, L-lysine is an ideal option.

4. Conclusions

The morphology of zeolite is one of the main factors that determine its catalytic, adsorption and separation performance. Therefore, the preparation of zeolite crystals with ideal morphology has always been the goal of researchers' efforts, and promising progress has been achieved. It has been shown that synthesis conditions have a great influence on the morphology of zeolite crystals, including the synthesis formula and its ratios, the crystallization temperature and time, and the synthesis method, because these factors significantly affect the nucleation and crystal growth rate of zeolites by altering or modifying the gelation and crystallization processes. To control the anisotropic growth of zeolites, the addition of morphology modifiers to the synthesized gel is one of the effective methods to obtain the desired zeolite crystal shape.

The strategies for manipulating MFI zeolite morphologies using organic modifiers are categorized and presented in this review. The use of urea solely or with a second additive, amino acids, small organic molecules (alcohols, N-compound, sugar, organic acids, and others) and polymers, was reviewed in detail. Various morphologies, including nanocrystals, aggregated nanoparticles, nanosheets, intergrown nanosheets, plates, intergrown plates, needles and bulky prismatic crystals were obtained using different additive types. Most of the studies were dedicated to preparing short-*b*-axis MFI type zeolites. The proposed potential role of additives in forming nanocrystals or nanosheets/plates is the adsorption of additive molecules on specific crystal facets, thus hindering further growth along that direction during the crystallization process. Applications using the different morphological MFI zeolites for catalytic reactions and separations were presented following each zeolite, showing superiors performance compared to that of the conventional MFI zeolite crystals, mainly due to the mitigation of diffusion

limitation along the specific crystallographic axis, of which the dimensions were prominently reduced.

Despite the successful synthesis of MFI zeolites with various morphologies, the role of most additives in directing certain morphologies remains elusive. Hence, rationale explanations based on sophisticated characterization (isotope-labelled experiments and *operando* spectroscopy) and simulations are necessary to fundamentally elucidate the growth mechanisms to provide guidelines for producing specific morphological MFI zeolites tailored to specific needs. Although the limitations of current characterization techniques and computation capacity do not allow us to directly investigate and explicitly illustrate such a complex system, we have reasons to believe that with scientific and technological advancements, the rational design of zeolite crystal morphology can be achieved in the future. Furthermore, cost efficiency should be considered to screen out practically viable additives to ensure the economical and scalable industrial production and use of the materials. Lastly, the potential pollution caused by organic additives during and after zeolite synthesis should also be considered since more stringent legislation is introduced on controlled carbon emissions and environmental protection.

Data availability

This article is a review article without any research data. All analysis results have been presented in the manuscript.

Author contributions

Jun Zhao: writing – review & editing – original draft, validation, investigation, formal analysis, and data curation. Haijun Yu: visualization, validation, conceptualization. Haimei Xu: software, methodology. Zhiyu He: discussion. Feng Shao: co-supervision. Peng Lu: writing – review & editing, supervision, project administration, funding acquisition. Valentin Valtchev: writing – review & editing, supervision, project administration, funding acquisition.

Conflicts of interest

There are no conflicts of interest to declare.

Acknowledgements

The ZeoMat Group acknowledges the starting grant provided by QIBEBT (Qingdao Institute of Bioenergy and Bioprocess Technology) and the support provided by the Shandong Energy Institute (SEI S202107). P. L. acknowledges the support by QIBEBT International Collaboration Program (202305) and by the Key Laboratory of Photoelectric Conversion and Utilization of Solar Energy (Innovation Fund Project No. KLPCU2024DP01).

Notes and references

1 C. J. Rhodes, *Sci. Prog.*, 2010, **93**, 223–284.
2 S. Montalvo, C. Huilinir, R. Borja, E. Sanchez and C. Herrmann, *Bioresour. Technol.*, 2020, **301**, 122808.
3 X. Chi, M. Li, J. Di, P. Bai, L. Song, X. Wang, F. Li, S. Liang, J. Xu and J. Yu, *Nature*, 2021, **592**, 551–557.
4 R. Ryoo, J. Kim, C. Jo, S. W. Han, J.-C. Kim, H. Park, J. Han, H. S. Shin and J. W. Shin, *Nature*, 2020, **585**, 221–224.
5 J. Shi, Y. Wang, W. Yang, Y. Tang and Z. Xie, *Chem. Soc. Rev.*, 2015, **44**, 8877–8903.
6 B. M. Weckhuysen and J. Yu, *Chem. Soc. Rev.*, 2015, **44**, 7022–7024.
7 B. Min, A. Korde, S. Yang, Y. Kim, C. W. Jones and S. Nair, *AIChE J.*, 2021, **67**, e17048.
8 C. S. Cundy and P. A. Cox, *Chem. Rev.*, 2003, **103**, 663–701.
9 G. T. Kokotailo, S. L. Lawton, D. H. Olson and W. M. Meier, *Nature*, 1978, **272**, 437–438.
10 T. C. T. Pham, T. H. Nguyen and K. B. Yoon, *Angew. Chem., Int. Ed.*, 2013, **52**, 8693–8698.
11 G. T. M. Kadja, M. D. Rukmana, R. R. Mukti, M. H. Mahyuddin, A. G. Saputro and T. D. K. Wungu, *Mater. Lett.*, 2021, **290**, 129501.
12 C. Zhang, S. Chu, J. Jiang, J. Zhao, S. Wen, B. Sun and W. Xu, *Front. Chem.*, 2022, **10**, 860795.
13 M. Liu, Z. Huang, W. Wei, X. Wang and Y. Wen, *Front. Chem.*, 2021, **9**, 682404.
14 B. Bensafi, N. Chouat and F. Djafri, *Coord. Chem. Rev.*, 2023, **496**, 215397.
15 R. Aiello, F. Crea, E. Nigro, F. Testa, R. Mostowicz, A. Fonseca and J. B. Nagy, *Microporous Mesoporous Mater.*, 1999, **28**, 241–259.
16 L. Zhang, Y. Song, G. Li, Q. Zhang, S. Zhang, J. Xu, F. Deng and Y. Gong, *RSC Adv.*, 2015, **5**, 61354–61363.
17 J. Dedecek, V. Balgova, V. Pashkova, P. Klein and B. Wichterlova, *Chem. Mater.*, 2012, **24**, 3231–3239.
18 K. A. Sashkina, Z. Qi, W. Wu, A. B. Ayupov, A. I. Lysikov and E. V. Parkhomchuk, *Microporous Mesoporous Mater.*, 2017, **244**, 93–100.
19 H. Li, X. Liu, S. Qi, L. Xu, G. Shi, Y. Ding, X. Yan, Y. Huang and J. Geng, *Angew. Chem., Int. Ed.*, 2017, **56**, 14090–14095.
20 M. Y. Jeon, D. Kim, P. Kumar, P. S. Lee, N. Rangnekar, P. Bai, M. Shete, B. Elyassi, H. S. Lee, K. Narasimharao, S. N. Basahel, S. Al-Thabaiti, W. Xu, H. J. Cho, E. O. Fetisov, R. Thyagarajan, R. F. DeJaco, W. Fan, K. A. Mkhoyan, J. I. Siepmann and M. Tsapatsis, *Nature*, 2017, **543**, 690–694.
21 G. Gwak, J.-h. Park and D. Kim, *Microporous Mesoporous Mater.*, 2023, **349**, 112424.
22 Y. Seo, S. Lee, C. Jo and R. Ryoo, *J. Am. Chem. Soc.*, 2013, **135**, 8806–8809.
23 K. Na, C. Jo, J. Kim, K. Cho, J. Jung, Y. Seo, R. J. Messinger, B. F. Chmelka and R. Ryoo, *Science*, 2011, **333**, 328–332.
24 L. Emdadi, Y. Wu, G. Zhu, C.-C. Chang, W. Fan, P. Trong, R. F. Lobo and D. Liu, *Chem. Mater.*, 2014, **26**, 1345–1355.
25 P. Rani, R. Srivastava and B. Satpati, *Cryst. Growth Des.*, 2016, **16**, 3323–3333.
26 Y. Liu, W. Qiang, T. Ji, M. Zhang, M. Li and J. Lu, *Sci. Adv.*, 2020, **6**, eaay5993.

27 Z. Qin, L. Pinard, M. A. Benghalem, T. J. Daou, G. Melinte, O. Ersen, S. Asahina, J.-P. Gilson and V. Valtchev, *Chem. Mater.*, 2019, **31**, 4639–4648.
28 J. Prech, K. N. Bozhilov, J. El Fallah, N. Barrier and V. Valtchev, *Microporous Mesoporous Mater.*, 2019, **280**, 297–305.
29 M. Choi, K. Na, J. Kim, Y. Sakamoto, O. Terasaki and R. Ryoo, *Nature*, 2009, **461**, 246–249.
30 W. Dai, C. Kouvatas, W. Tai, G. Wu, N. Guan, L. Li and V. Valtchev, *J. Am. Chem. Soc.*, 2021, **143**, 1993–2004.
31 C. Wang, W. Fang, Z. Liu, L. Wang, Z. Liao, Y. Yang, H. Li, L. Liu, H. Zhou, X. Qin, S. Xu, X. Chu, Y. Wang, A. Zheng and F.-S. Xiao, *Nat. Nanotechnol.*, 2022, **17**, 714–720.
32 J. Duan, W. Chen, C. Wang, L. Wang, Z. Liu, X. Yi, W. Fang, H. Wang, H. Wei, S. Xu, Y. Yang, Q. Yang, Z. Bao, Z. Zhang, Q. Ren, H. Zhou, X. Qin, A. Zheng and F.-S. Xiao, *J. Am. Chem. Soc.*, 2022, **144**, 14269–14277.
33 J. Yang, K. Gong, D. Miao, F. Jiao, X. Pan, X. Meng, F. Xiao and X. Bao, *J. Energy Chem.*, 2019, **35**, 44–48.
34 Z. Liu, D. Wu, S. Ren, X. Chen, M. Qiu, X. Wu, C. Yang, G. Zeng and Y. Sun, *ChemCatChem*, 2016, **8**, 3317–3322.
35 M. Zhang, S. Ren, Q. Guo and B. Shen, *ChemistrySelect*, 2023, **8**, e202203687.
36 J. Zhu, S. Yan, G. Xu, X. Zhu and F. Yang, *J. Solid State Chem.*, 2023, **318**, 123772.
37 X. Lv, M. Yang, S. Song, M. Xia, J. Li, Y. Wei, C. Xu, W. Song and J. Liu, *ACS Appl. Mater. Interfaces*, 2023, **15**, 14250–14260.
38 Q. Yue, C. Liu, H. Zhao, H. Liu, P. Ruterana, J. Zhao, Z. Qin and S. Mintova, *Nano Res.*, 2023, **16**, 12196–12206.
39 J. Shi, Y. Du, W. He, G. Zhao, Y. Qin, L. Song, J. Hu, Y. Guan, J. Zhu, C. Wang, J. Teng and Z. Xie, *Chem.–Eur. J.*, 2022, **28**, e202201781.
40 J. Xu, Z. Zhang, D. Yu, W. Du, N. Song, X. Duan and X. Zhou, *Nano Res.*, 2023, **16**, 6278–6289.
41 Z. Shan, H. Wang, X. Meng, S. Liu, L. Wang, C. Wang, F. Li, J. P. Lewis and F.-S. Xiao, *Chem. Commun.*, 2011, **47**, 1048–1050.
42 C. Ping, Q. Zhu, W. Ma, C. Hu and Y. Zhang, *J. Porous Mater.*, 2022, **29**, 1919–1928.
43 Y. Liu, X. Zhou, X. Pang, Y. Jin, X. Meng, X. Zheng, X. Gao and F.-S. Xiao, *ChemCatChem*, 2013, **5**, 1517–1523.
44 B. A. Qureshi, X. Lan, M. T. Arslan and T. Wang, *Ind. Eng. Chem. Res.*, 2019, **58**, 12611–12622.
45 B. Ali, X. Lan, M. T. Arslan, S. Z. A. Gilani, H. Wang and T. Wang, *J. Ind. Eng. Chem.*, 2020, **88**, 127–136.
46 Y. Ma, Z. Li, N. Zhao, F. Han and Q. Kan, *Nano*, 2020, **15**, 2050026.
47 X. Song, X. Yang, T. Zhang, H. Zhang, Q. Zhang, D. Hu, X. Chang, Y. Li, Z. Chen, M. Jia, P. Zhang and J. Yu, *Inorg. Chem.*, 2020, **59**, 13201–13210.
48 W. Qin, A. Agarwal, M. K. Choudhary, J. C. Palmer and J. D. Rimer, *Chem. Mater.*, 2019, **31**, 3228–3238.
49 Q. Zhang, G. Chen, Y. Wang, M. Chen, G. Guo, J. Shi, J. Luo and J. Yu, *Chem. Mater.*, 2018, **30**, 2750–2758.
50 R. Watanabe, T. Yokoi and T. Tatsumi, *J. Colloid Interface Sci.*, 2011, **356**, 434–441.
51 S. Peng, G. Yang and J. Zhang, *Inorg. Chem. Commun.*, 2022, **143**, 109759.
52 Y.-Q. Deng, S.-F. Yin and C.-T. Au, *Ind. Eng. Chem. Res.*, 2012, **51**, 9492–9499.
53 X. Chen, W. Yan, X. Cao, J. Yu and R. Xu, *Microporous Mesoporous Mater.*, 2009, **119**, 217–222.
54 X. Liu, J. Shi, G. Yang, J. Zhou, C. Wang, J. Teng, Y. Wang and Z. Xie, *Commun. Chem.*, 2021, **4**, 107.
55 P. Zhu, J. Wang, F. Xia, W. Zhang, H. Liu and X. Zhang, *Eur. J. Inorg. Chem.*, 2023, **26**, e202200664.
56 A. I. Lupulescu and J. D. Rimer, *Angew. Chem., Int. Ed.*, 2012, **51**, 3345–3349.
57 P. Wang, X. Xiao, Y. Pan, Z. Zhao, G. Jiang, Z. Zhang, F. Meng, Y. Li, X. Fan, L. Kong and Z. Xie, *Catalysts*, 2022, **12**, 351.
58 L. Liu, H. Wang, R. Wang, C. Sun, S. Zeng, S. Jiang, D. Zhang, L. Zhu and Z. Zhang, *RSC Adv.*, 2014, **4**, 21301–21305.
59 Z. Shang, Y. Chen, L. Zhang, X. Zhu, X. Wang and C. Shi, *Inorg. Chem. Front.*, 2022, **9**, 1456–1466.
60 Z. Shang, Y. Chen, L. Zhang, X. Zhu, X. Wang and C. Shi, *Inorg. Chem. Front.*, 2022, **9**, 2097–2103.
61 Y. Rong, X. Zhang, H. Wang, D. Tan, H. Wang and T. Zhang, *Microporous Mesoporous Mater.*, 2022, **341**, 112094.
62 R. Feng, X. Wang, J. Lin, Z. Li, K. Hou, X. Yan, X. Hu, Z. Yan and M. J. Rood, *Microporous Mesoporous Mater.*, 2018, **270**, 57–66.
63 R. Feng, X. Yan, X. Hu, J. Wu and Z. Yan, *Microporous Mesoporous Mater.*, 2020, **302**, 110246.
64 J. Shi, G. Zhao, J. Teng, Y. Wang and Z. Xie, *Inorg. Chem. Front.*, 2018, **5**, 2734–2738.
65 X. Wang, P. Karakiliç, X. Liu, M. Shan, A. Nijmeijer, L. Winnubst, J. Gascon and F. Kapteijn, *ACS Appl. Mater. Interfaces*, 2018, **10**, 33574–33580.
66 Y. Yang, X. Lu, H. Zhang, X. Yu, Q. Zheng and Z. Wang, *Chem.–Asian J.*, 2023, **18**, e202300218.
67 Z. Zhou, R. Jiang, X. Chen, X. Wang and H. Hou, *J. Solid State Chem.*, 2021, **298**, 122132.
68 X. Chen, R. Jiang, Z. Zhou and X. Wang, *J. Dispersion Sci. Technol.*, 2021, **42**, 561–568.
69 Y. Ji, Y. Zuo, M. Liu, F. Wang, C. Song and X. Guo, *Microporous Mesoporous Mater.*, 2021, **321**, 111100.
70 L. Guo, Z. Wang, J. Wang, Z. Wang, S. Xue, X. Jiang, T. Lu, J. Xu, Y. Zhan and L. Han, *J. Sol-Gel Sci. Technol.*, 2020, **96**, 256–263.
71 G. Lv, S. Deng, Y. Zhai, Y. Zhu, H. Li, F. Wang and X. Zhang, *Appl. Catal., A*, 2018, **567**, 28–35.
72 B. Zhang, Y. Shao, T. Tatsumi and J. Wang, *Mater. Lett.*, 2022, **317**, 132076.